

Simulations of Mixed Morphology Supernova Remnants With Anisotropic Thermal Conduction

David A. Tilley^{*}, Dinshaw S. Balsara and J. Christopher Howk

Department of Physics, University of Notre Dame, Notre Dame, Indiana 46556 USA

5 October 2018

ABSTRACT

We explore the role of anisotropic thermal conduction on the evolution of supernova remnants through interstellar media with a range of densities via numerical simulations. We find that a remnant expanding in a dense environment can produce centre-bright hard x-ray emission within 20 kyr, and centre-bright soft x-ray emission within 60 kyr of the supernova event. In a more tenuous environment, the appearance of a centre-bright structure in hard x-rays is delayed until about 60 kyr. The soft x-ray emission from such a remnant may not become centre bright during its observable lifetime. This can explain the observations that show that mixed-morphology supernova remnants preferentially occur close to denser, molecular environments. Remnants expanding into denser environments tend to be smaller, making it easier for thermal conduction to make larger changes in the temperatures of their hot gas bubbles. We show that the lower temperatures make it very favorable to use high-stage ions as diagnostics of the hot gas bubbles in SNRs. In particular, the distribution of O VIII transitions from shell-bright at early epochs to centre-bright at later epochs in the evolution of an SNR expanding in a dense ISM when the physics of thermal conduction is included.

Key words: conduction – MHD – supernova remnants – X-rays: ISM – ISM: magnetic fields

1 INTRODUCTION

Supernovae play an important role in driving the thermal evolution of the interstellar medium (ISM henceforth). The interiors of supernova remnants (SNR henceforth) are filled with extremely hot plasma, with temperatures of 10^6 – 10^7 K. The classical picture of the expansion of a supernova remnant into the interstellar medium identifies four stages that are still germane today (see Woltjer 1972). At very early times, the remnant is freely expanding into the undisturbed medium. After the shock sweeps up more mass than was ejected by the supernova, the remnant expands adiabatically according to the Sedov (1959) solution. When the cooling time of the matter behind the shock becomes comparable to the dynamical time of the expansion, a cold, dense shell is formed. Eventually, the expansion velocity of the shock becomes comparable to the turbulent velocity in the ISM, and the remnant disperses.

SNRs can be classified into several morphological types; see Weiler & Sramek (1988) and Jones et al. (1998) for excellent reviews. The classical or shell-type SNRs are the most

common and are shell-bright in both x-rays and radio emission. The former arises from thermal bremsstrahlung and inner-shell metal line emission in the hot gas behind the shock. Synchrotron emission from cosmic rays and magnetic field swept up by the shock leads to the radio morphology. Plerionic remnants are powered by a central pulsar and have bright, nonthermal radio emission in their interior. Finally, there is a composite class, including radio and x-ray composite morphologies, which exhibit both a radio-bright shell and centre-bright x-ray emission. The x-ray composite remnants (also known as thermally composite or mixed morphology, MM henceforth) comprise 8 per cent of all remnants (Rho & Petre 1998).

Rho & Petre also found that MM SNRs preferentially occur toward the Galactic midplane where the gas is denser. Rho & Petre cite Frail et al. (1996); Reach & Rho (1996); Koo & Moon (1997) to demonstrate that the shocks from MM SNRs could be interacting with molecular cloud material, suggesting that MM SNRs occur in denser environments. In this paper, we examine that hypothesis. Kawasaki et al. (2005) have proposed all SNRs pass through a composite phase. Their argument is based on over-ionisation in the majority of MM SNRs. We examine the

^{*} E-mail: dtolley@nd.edu (DAT); dbalsara@nd.edu (DSB); jhowk@nd.edu (JCH)

hypothesis that all SNRs pass through an MM phase with our simulations.

Two existing models for the formation of MM SNRs have figured prominently since the recognition of this class of remnant. The first model, proposed by White & Long (1991), has cool, dense clouds that become engulfed by the supernova shock and hot gas bubble. Thermal conduction and turbulent mixing transfer heat between the bubble and clouds, cooling the interior of the SNR and increasing its density as the cold gas in the clouds evaporates and mixes with the remnant.

The second model by Cox et al. (1999) proposed that thermal conduction acting by itself can cause a SNR to become centre-bright in x-rays if the remnant is expanding into a dense medium. As the sound speed of the thermal electrons is significantly greater than the sound speed of the ions, the electrons can propagate faster than the outer shock and carry energy away from the interior. The interior density increases as the bubble cools (Slavin & Cox 1992; Cox et al. 1999; Shelton et al. 1999). The transport of heat from the hot interior of the remnant to the surrounding medium leads to lower temperatures and higher densities inside the SNR, leading to greater emission in x-rays from the centre of the remnant.

In each of these models, thermal conduction is invoked to transport energy from the hot gas to cool gas. They differ primarily in how they distribute the cold, dense gas component. In either of these scenarios, the higher densities and cooler temperatures of $10^5 - 10^6$ K in the hot gas bubble favor the production of soft x-rays in the centres of these remnants. We concentrate on the latter model in this work.

In the presence of a magnetic field, thermal conduction becomes anisotropic as the free electrons that are responsible for the bulk of the heat transport will not propagate further than the Larmor radius of the magnetic field (Spitzer 1956; Cowie & McKee 1977; Balbus 1986). Thus, the geometry of the magnetic field cannot be neglected when calculating the thermal heat flux in a multidimensional calculation. As a result, Tilley & Balsara (2006) examined the role of anisotropic thermal conduction in the presence of magnetic fields and showed that it is important in determining the filling factor of hot gas in our Galaxy.

Slavin & Cox (1992, 1993) used a simplified representation of the magnetic field in their early calculations and we improve on that here. Velázquez et al. (2004) include the anisotropy in the thermal conduction introduced by the magnetic field, but do not include the Lorentz force of the magnetic field on the gas. As a consequence, the magnetic field was stirred by the turbulent motions developing behind the supernova shock, greatly inhibiting thermal conduction. Without the feedback of the magnetic field on the gas, however, this can only be regarded as a lower limit on the degree of thermal conduction. We removed this restriction in Tilley & Balsara (2006), and here we examine further consequences of removing that restriction.

A goal of our work, with its limited but interesting set of input micro-physics, is to produce diagnostics that may be compared with observations. Recent work by the *FUSE*, *Chandra* and *XMM* observatories have provided insight into the total amount of hot gas in the Galaxy, as traced by highly-ionised stages of oxygen, esp. O VI and O VIII (Oegerle 2005; Yao & Wang 2005; Savage & Lehner 2006).

Table 1. Initial conditions of the ISM in our simulations. ρ is the density in amu cm $^{-3}$; T is the temperature in Kelvin; B is the magnetic field in μ G; and L is the grid size in parsecs.

Run	ρ	T	B	L
L0	0.7	8000	0.0	75
L1	0.7	8000	3.0	75
M0	1.0	10000	0.0	50
M1	1.0	10000	3.0	50
H0	5.0	10000	0.0	50
H1	5.0	10000	6.0	50

These ions probe gas in the temperature range $\sim 10^5$ K to $\sim 10^8$ K, providing valuable diagnostics of the thermal state of the hot material in the Milky Way. While such data have so far been used to test global models of the ISM (McKee & Ostriker 1977; Korpi et al. 1999; Kim et al. 2001; de Avillez & Breitschwerdt 2004; Balsara et al. 2004; Balsara & Kim 2005; Avillez & Breitschwerdt 2005; Mac Low et al. 2005; Tilley & Balsara 2006), it is also possible to use high-stage ions as diagnostics for the structure of SNRs. Indeed, while earlier observatories allowed spectroscopy of small regions of supernova remnants (e.g., Vedder et al. 1986), recent *Chandra* and *XMM* observations have provided spatially-resolved measurements of O VII and O VIII emission from SNRs (Gaetz et al. 2000; Rasmussen et al. 2001; van der Heyden et al. 2002; Flanagan et al. 2004). We further develop the idea of using high-stage ions as diagnostics of hot gas in SNRs in this paper.

In this paper we report on the results of a series of MHD simulations on the evolution of SNRs with anisotropic thermal conduction. We explore a parameter space of initial ISM conditions in density, temperature, and magnetic field strength (Section 2). In Section 3 we analyse the effects of the environment on the evolution of the remnant, in particular focusing upon the effects of the environment on producing mixed-morphology remnants. Section 4 explores the role that high-stage ions could play in diagnosing the hot gas. Section 5 provides some conclusions.

2 NUMERICAL SETUP

We carried out our simulations by using the RIEMANN code (Roe & Balsara 1996; Balsara 1998a,b; Balsara & Spicer 1999a,b; Balsara 2001, 2004). RIEMANN updates the MHD equations using a second-order accurate dimensionally unsplit TVD scheme. We use an implicit solver for the thermal conduction. We discuss the details of our treatment of anisotropic thermal conduction in an accompanying paper (Balsara et al., in preparation). We draw on Spitzer (1956); Cowie & McKee (1977); Balbus (1986); Slavin & Cox (1992) for our description of the classical thermal conduction flux, which is proportional to a temperature-dependent conductivity and the projection of the thermal gradient on to the local magnetic field:

$$\mathbf{F}_{\text{clas}} = -aT^{5/2}\hat{\mathbf{b}}(\hat{\mathbf{b}} \cdot \nabla T) \quad (1)$$

where T is the temperature, $a = 6 \times 10^{-7}$ g cm $^{-3}$ s $^{-3}$ K $^{-7/2}$ and $\hat{\mathbf{b}} = \mathbf{B}/|\mathbf{B}|$ is a unit vector along the magnetic field. When the flux becomes saturated, it no longer depends on

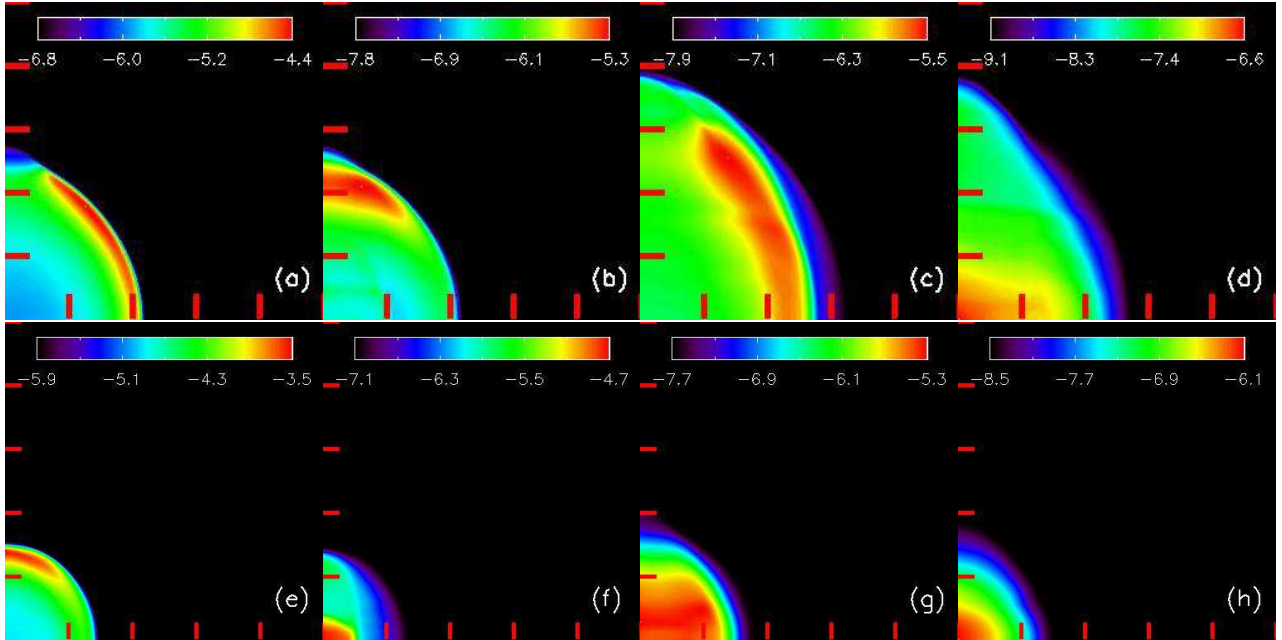


Figure 1. Simulated x-ray surface brightness in soft and hard x-rays, as described in the text. (a) and (b) show soft and hard x-rays from Run L1 (low-density ISM) at 20 kyr. (c) and (d) do the same for Run L1 at 60 kyr. (e) and (f) show soft and hard x-rays from Run H1 (high-density ISM) at 20 kyr, while (g) and (h) show the same for Run H1 at 60 kyr. The tick marks indicate projected distances of 10 pc. The colour scale is the logarithm of the surface brightness in $\text{ergs s}^{-1} \text{ cm}^{-2} \text{ sr}^{-1}$.

the value of the temperature gradient, only on the presence of a parallel component of the temperature gradient to the magnetic field (Balbus 1986):

$$F_{\text{sat}} = -5\phi\rho c_s^3 \text{sgn}(\hat{\mathbf{b}} \cdot \nabla T) \hat{\mathbf{b}} \quad (2)$$

where c_s is the sound speed, ρ the density and $\phi \sim 0.3$ (Balbus & McKee 1982). A flux limiter is utilized to transition from the classical flux to the saturated flux (Balbus & McKee 1982; Slavin & Cox 1992). The transition from the classical (Eq. 1) to saturated (Eq. 2) thermal conduction causes the flux to change character from parabolic to hyperbolic (Balbus 1986). The changing character in the flux of thermal conduction is accounted for by using a Newton-Krylov multigrid method that correctly incorporates the anisotropic structure of the thermal conduction operator in the presence of a magnetic field. We have tested our formulation of the thermal conduction against the supernova shock radius-time relation of Cioffi et al. (1988) and found excellent agreement. We also found very good agreement with the instability growth rates predicted by Field (1965). These tests are described in detail in (Balsara et al., in preparation).

Radiative cooling is calculated using the cooling function of MacDonald & Bailey (1981). We balance the cooling rate of our initial conditions with a constant heating rate, such that the initial conditions would remain at constant temperature in the absence of the supernova remnant. Our choice of equilibrium cooling permits us to do a large number of runs without carrying the large number of species that would be necessary in a formulation that retains the non-equilibrium ionisation (Slavin & Cox 1992). However, more economical formulations for the inclusion of non-equilibrium cooling are becoming available (Benjamin et al. 2001) and it is our intent to incorporate such physics in future mod-

els. The focus of our present paper is to examine the role of thermal conduction, which does not depend sensitively on the details of the radiative cooling.

We use a uniform mesh in cylindrical coordinates of 384x384 zones in the R-z plane to update the MHD equations. We chose our initial densities and temperatures of the quiescent environment so that they are representative of interesting interstellar medium conditions. Our lowest density runs, labelled ‘‘L0’’ and ‘‘L1’’, have a density of 0.7 amu cm^{-3} , a temperature of 8000 K and a magnetic field of $0 \mu\text{G}$ and $3 \mu\text{G}$, respectively. Our intermediate runs, labelled ‘‘M0’’ and ‘‘M1’’, have a density of 1.0 amu cm^{-3} , a temperature of 10000 K and a magnetic of $0 \mu\text{G}$ and $3 \mu\text{G}$, respectively. Our highest density runs, labelled ‘‘H0’’ and ‘‘H1’’, have a density of 5.0 amu cm^{-3} , a temperature of 10000 K and a magnetic field of $0 \mu\text{G}$ and $6 \mu\text{G}$, respectively. These initial conditions are summarized in Table 1. In all of these cases, we initialize our supernova with 10^{51} ergs of energy, partitioned such that one-third of the supernova energy is contained in thermal energy, and the other two-thirds in kinetic energy. We initialize our remnant with a radius of 10 zones in all of our simulations. In order to follow the complete evolution of the remnant, we wish to ensure that the outer shock remains on the grid at all times. The physical size of our grid in each of the simulations in Table 1 reflects this. To serve as a counterpoint we have carried out a complementary set of simulations without thermal conduction, but including radiative cooling.

3 MIXED MORPHOLOGY REMNANTS

The structure of supernova remnants that include anisotropic thermal conduction in magnetized ISMs has

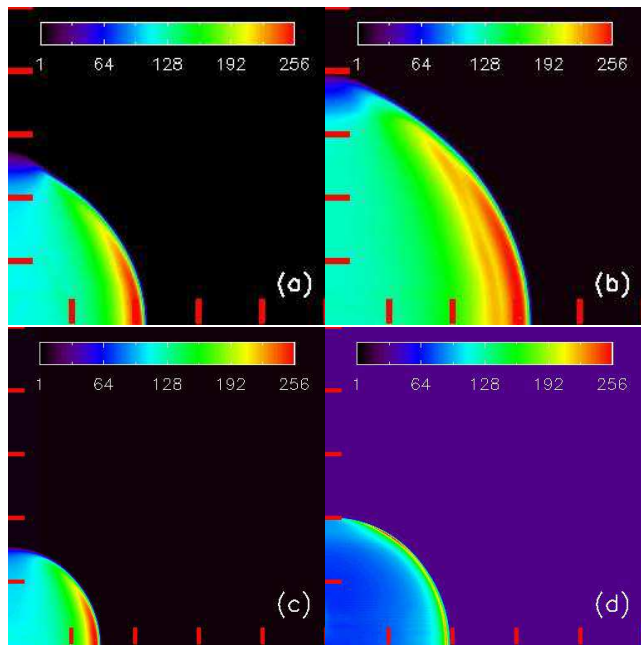


Figure 2. Simulated synchrotron surface brightness $\propto PB^{1.5}$ from SNRs, shown at two epochs, (Left) 20 kyr after the explosion. (Right) 60 kyr after the explosion. The top row illustrates the expansion of a SNR into a standard ISM (Run L1). The bottom row illustrates the expansion of a SNR into a higher-density ISM (Run H1). The tick marks indicate projected distances of 10 pc. Units on the linear colour scale are arbitrary, and scaled such that the greatest surface brightness has a value of 256.

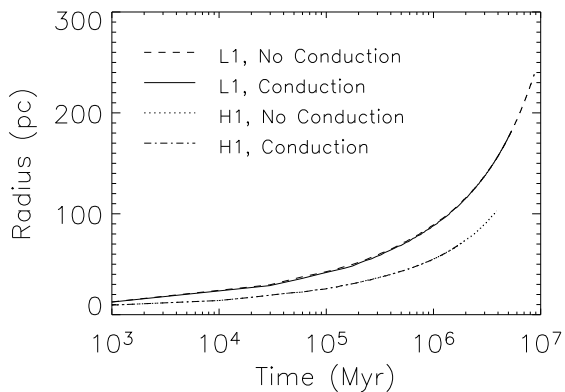


Figure 3. Radius of the outer shock as it evolves with time, showing the difference in the evolution between runs with and without conduction, and runs in low or high density ISMs. The solid and dashed lines virtually overlap each other. Likewise, the dotted and dot-dashed lines also practically overlap each other.

been studied in Tilley & Balsara (2006). In their fig. 1, they intercompare remnants that include thermal conduction to those that exclude thermal conduction, but in both cases they incorporate the effects of radiative cooling. In the snowplow phase, they find that the temperature of the hottest gas is reduced by a factor of ~ 10 , while the density is increased by the same factor, in those remnants that include thermal conduction. They also find that the inclusion of a uniform

magnetic field restricts the thermal conduction in the direction of the magnetic field. As a consequence, the structure of the hot gas bubble becomes elongated in the direction of the magnetic field.

MM SNRs are primarily diagnosed in x-ray and radio emission. Moreover, *Chandra* has made it possible to image the same remnant in soft and hard x-rays with high spatial resolution. To examine the influence of thermal conduction on the production of the morphology of the remnant at these energies, we produce simulated emission maps of our models at several epochs during the course of the SNR's evolution. We calculate the x-ray emissivity for $10^5 - 10^8$ K gas using Raymond & Smith (1977). These emissivities include the contribution from bremsstrahlung, high-order atomic lines, recombination and two-photon emission for photons in the range of 100 eV - 10 keV. We then integrated the optically thin emission along the line-of-sight to create projected intensity maps of the simulated SNRs in x-rays.

The projected soft and hard x-ray maps are shown in Fig. 1. To retain some concordance with *Chandra* data, we define 'soft x-rays' as those with photon energies in the range of 300-800 eV, and 'hard x-rays' as those with energies in the range of 1-5 keV. The resultant images were not convolved with an instrumental spatial or spectral response function. Fig. 1 (a) and (b) show the soft and hard x-rays in the low-density run L1 at 20 kyr. Fig. 1 (c) and (d) do the same at 60 kyr. Fig. 1 (e) through (h) show similar data for the high-density run H1 at the same epochs. Fig. 1 (a) and (b) show that at early epochs, the low-density run L1 is shell-bright in soft x-rays, and also shell-bright in hard x-rays. The magnetic field draws heat from the hottest central gas and carries it to the pole, making Fig. 1(b) brighter at the pole, while Fig. 1(a) is brighter at the equator. Fig. 1 (e) and (f) show that at 20 kyr the high-density run H1 is shell-bright in the soft x-rays, but is already centre-bright in the hard x-rays. Shelton et al. (1999) also present simulated hard x-ray images of remnants expanding into an unmagnetized medium of similar density, finding that they too produce centre-bright images in the hard x-ray and thereby producing a concordance between our data and theirs.

At later epochs, i.e. 60 kyr, Fig. 1 (c) and (d) show that the low-density run L1 is still shell-bright in soft x-rays, but is becoming centre-bright in hard x-rays. Fig. 1 (g) and (h) show that the high-density run H1 has become centre-bright in both soft and hard x-rays. This shows that thermal conduction plays an important role in making model H1 centre-bright in x-rays. A similar conclusion emerges when we cross-compare models L0 and H0 without magnetic fields. The difference between models that include magnetic fields and those that exclude it is that without magnetic fields thermal conduction operates in both the R and z directions, thereby increasing the rate at which energy is transported from the hot gas bubble. As a result, thermally conducting remnants that exclude magnetic fields make their transition to a centre-bright x-ray morphology at an earlier epoch.

The morphological differences between Fig. 1 (a) and (b) require further explanation. The anisotropy in the thermal conduction flux caused by the presence of the magnetic field leads to the incomplete appearance of the shell. Temperature variations perpendicular to the field are not reduced due to thermal conduction. As the magnetic field is swept up by the SNR, the magnetic flux becomes concen-

trated in a thin shell. Most of the magnetic field in the interior of the remnant nevertheless retains some memory of its original orientation. As a result, it is preferentially attached to the exterior medium closer to the z-axis. Consequently, the outer regions of the hot bubble near the axis of symmetry have a lower density and higher temperature than the outer parts of the bubble near the midplane, resulting in lower emission in soft x-rays and a higher emission in hard x-rays near the pole at early epochs. A remnant going off into a denser medium is smaller and reaches its snowplow phase faster. As a result, thermal conduction is more efficient at transferring energy within such a remnant. For that reason, we see that H1 has already become centre-bright in hard x-rays, with the soft x-rays showing an incomplete shell, see Fig. 1(e) and (f). We see, therefore, that the choice of wavebands used to image the remnant can also make a difference in its classification as a centre-bright remnant in x-rays. In particular, remnants expanding into a denser ISM would be much more likely to be classified as centre-bright if they are imaged in hard x-rays instead of soft x-rays.

Magnetic fields are compressed by the outer shock in an SNR, and can even be amplified if the shock interacts with interstellar turbulence (Balsara et al. 2001). Cosmic rays can also be swept up by the outer shock and are most likely accelerated by it. We do not include cosmic ray acceleration processes here. As a result, we calculate synchrotron emissivities as $\epsilon_{\text{synch}} \propto PB^{1.5}$ (see Clarke et al. 1989; Jun & Jones 1999). The simulated synchrotron maps are illustrated in Fig. 2. In both the high-density and low-density environments the concentrated magnetic field appears as a bright shell behind the shock at all times. Thus, we find a clear difference between the morphological appearance at 60 kyr in x-rays and radio emission.

The previous paragraph has shown us that the radio morphology is always shell-bright. We have also seen that the transition to a centre-bright x-ray morphology depends to some extent on the wavebands used. If we use soft x-rays, we find that remnants expanding into a denser environment enter a mixed-morphology phase within about 60 kyr, while remnants expanding into a standard ISM do not transition to a mixed morphology within that time. However, even the remnants expanding into a standard ISM do transition to a mixed morphology after about 90 kyr. This might, however, be too late in the life of a remnant for it to be visible. We note that the soft x-ray flux has already decreased by an order of magnitude between Fig. 1(a) and Fig. 1(c). We expect it to decrease by a similar magnitude by 90 kyr. If we use hard x-rays, we find that the remnant expanding into a denser environment is already centre-bright by about 20 kyr, while the remnant expanding into a standard ISM does not become centre-bright until about 60 kyr. We see, therefore, that the classification as a mixed-morphology remnant might depend strongly on the waveband used. We can, nevertheless, say with confidence that remnants expanding into denser ISMs might spend a significant fraction of their observable lives as mixed-morphology remnants. We cannot say the same for remnants expanding into a standard ISM. As a result, we conclude that the conjecture in Kawasaki et al. (2005), that all remnants pass through a mixed-morphology phase in their evolution, may in theory be quite plausible. However, remnants expanding into ISMs with standard densities or below-average densities may not

display themselves as mixed-morphology remnants during a significant phase of their observable lifetimes.

It is also important to realize that thermal conduction does not reduce the total energy, it only transports it from one place to another. Consequently, our numerical formulation is also fully conservative. Fig. 3 shows the location of the outer shock along the R-axis as a function of time. There is clearly no difference in the size of the shock whether thermal conduction is included or not. Since the location of the outer shock (at least in the radial direction) is unaffected by thermal conduction, we can conclude that the post-shock pressure should be the same in runs with and without conduction. The interior of the hot gas bubble is always hot enough (and the sound speed in it high enough) to ensure that the bubble achieves pressure balance with the post-shock gas. In the presence of thermal conduction the hot gas bubble can transport part of its thermal energy to some of the swept-up post-shock gas. This process can, therefore, lower the temperature in the hot gas bubble. To maintain constancy of pressure, the density in the hot gas will be correspondingly higher.

4 HIGH-STAGE IONS AS DIAGNOSTICS OF THE HOT GAS

In this Section, we examine the role of high-stage ions as diagnostics of hot gas in SNRs. Highly-ionised oxygen is readily observed in X-rays (e.g., through the O VII “triplet” at 21.60, 21.80, and 22.09 Å and O VIII Lyman- α at 18.98 Å) and in the far-ultraviolet (using the O VI doublet at 1033.8 Å). We will calculate the emission from these ions which probe a range of temperatures (O VI peaks at $\sim 3 \times 10^5$ K, O VII at $2.8 \times 10^5 - 1.8 \times 10^6$ K, and O VIII at $\sim 2.2 \times 10^6$ K). Thus, these ions provide good diagnostics of gas in these temperature regimes, which are important during the remnant evolution.

We use the line emissivity calculations from the Astrophysical Plasma Emission Code (APEC; Smith et al. 2001) with atomic data from the Astrophysical Plasma Emission Database (APED) included in the ATOMDB distribution (v. 1.3.1).¹ These calculations assume collisional ionisation equilibrium (Mazzotta et al. 1998), and we adopt an abundance of $\log \text{O/H} = -3.34$ from the solar system (Asplund et al. 2004). In what follows, O VI emission represents the sum of the O VI doublet emission, while O VII refers to the summed emission from the aforementioned triplet; O VIII emission refers to Lyman- α 18.98 Å emission. We have tested the temperature-dependent line emissivities from the APEC models using a treatment of O VI emission following Shull & Slavin (1994), and we find very good agreement.

Fig. 4 and 5 show maps of O VI, O VII, and O VIII at various epochs in simulations of SNRs going through low and high density ISMs. The results shown in Fig. 4 include thermal conduction. The results in Fig. 5 do not include thermal conduction. In each instance we show simulated images of O VI, O VII, and O VIII from left to right. Fig. 4(a) and Fig. 5(a) show these data in the low-density run at 20 kyr, and Fig. 4(b) and Fig. 5(b) show the same simulation at 60

¹ Available via <http://cxc.harvard.edu/atomdb/>.

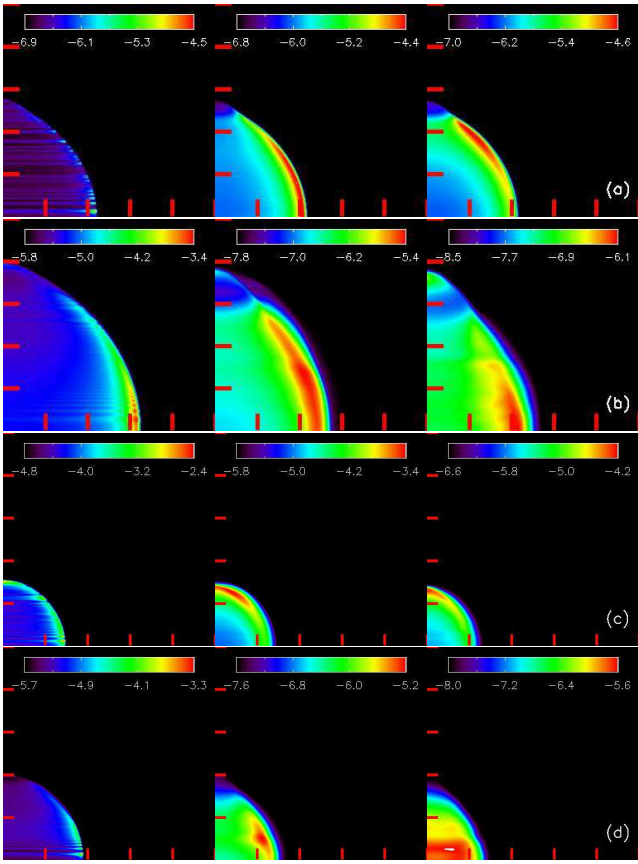


Figure 4. Surface brightness due to emission from oxygen ions for (a) Run L1 at 20 kyr, (b) Run L1 at 60 kyr, (c) Run H1 at 20 kyr, and (d) Run H1 at 60 kyr. The ions are (left) O VI, (centre) O VII, and (right) O VIII. The tick marks indicate projected distances of 10 pc. Because the distribution of O VI emitting gas originates from a very narrow shell, the image shows striations that arise from the pixellation of this boundary in the simulations. The colour scale is the logarithm of the surface brightness in $\text{ergs s}^{-1} \text{cm}^{-2} \text{sr}^{-1}$.

kyr. Similarly, Fig. 4(c) and Fig. 5(c) show these data in the high-density run at 20 kyr, and Fig. 4(d) and Fig. 5(d) show the same simulation at 60 kyr.

We see that O VI is always concentrated at the boundary of the hot gas bubble, thereby showing its utility as a tracer of the gas that it transitional between the hot and cold phases, and as a tracer of turbulent mixing layers as shown by Borkowski et al. (1990); Begelman & McKee (1990). The O VII shows itself to be shell-bright in all instances, with and without thermal conduction, indicating that it is not a good tracer of the role of thermal conduction in SNRs. Physically, this may be due to the broad range of temperatures over which O VII is the dominant ionisation stage of oxygen. By contrast, O VIII probes a narrow range of higher temperatures, and the distribution of O VIII is most interesting. Fig. 4(d) shows that the O VIII is centrally brightened at later stages in the evolution of the SNR when thermal conduction is included. This trend occurs to a lesser extent in Fig. 4(b), with more O VIII emission arising in the central region when thermal conduction is included. Fig. 5(b) and (d) show a strongly edge-brightened appearance in O VIII, even at late epochs, when thermal conduction is not

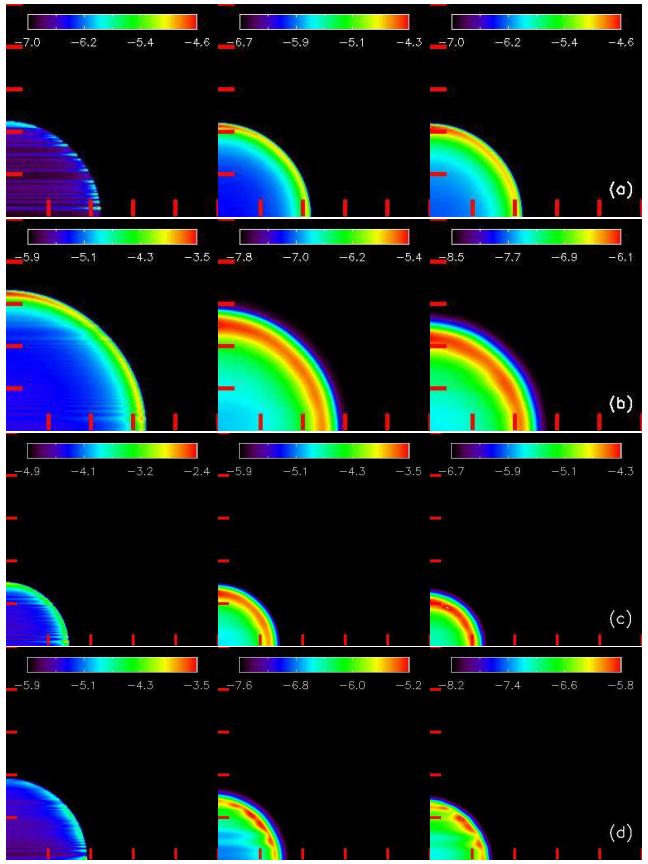


Figure 5. Surface brightness due to emission from oxygen ions for simulations without thermal conduction. (a) Run L1 at 20 kyr, (b) Run L1 at 60 kyr, (c) Run H1 at 20 kyr, and (d) Run H1 at 60 kyr. The ions are (left) O VI, (centre) O VII, and (right) O VIII. The tick marks indicate projected distances of 10 pc. Because the distribution of O VI emitting gas originates from a very narrow shell, the image shows striations that arise from the pixellation of this boundary in the simulations. The colour scale is the logarithm of the surface brightness in $\text{ergs s}^{-1} \text{cm}^{-2} \text{sr}^{-1}$.

included. Thus, thermal conduction plays an important role in cooling down the interior of the hot gas bubble at late epochs. This changes the ionisation balance, driving the interior from O IX to O VIII and making the centre of the remnant brighter in O VIII. Comparing Fig. 4 with Fig. 5, we see that thermal conduction played a major role in making the SNRs centre bright in O VIII at later epochs in dense ISMs. Our simulations therefore demonstrate the utility of using O VIII as a diagnostic of remnant age. We hasten to point out that our present conclusions for the high-stage ions are limited by our use of equilibrium cooling. The ionisation fractions of the different oxygen ions could change in the presence of non-equilibrium physics, and a future round of simulations will examine whether this trend is preserved when such physics are included.

5 CONCLUSION

Anisotropic thermal conduction decreases the average temperature of hot gas by half an order of magnitude over a period of a few million years, and increase the mean den-

sity by a similar amount. The temperature in the hottest portions of the hot gas bubble is reduced by an entire order of magnitude when thermal conduction is included, with a corresponding increase in the density. These changes affect the emission in high-stage ions rather strongly. In particular, the distribution of O VIII in a denser ISM transitions from shell-bright at early epochs to centre-bright at later epochs when the physics of thermal conduction is included.

In denser ISMs (such as in proximity to giant molecular clouds, in the bulges of spiral galaxies and in starburst galaxies) the higher density and lower temperatures lead to the development of centre-bright soft x-ray emission at late stages in the evolution of the SNR. This confirms that it is possible to produce MM SNRs in denser environments through the process of thermal conduction alone. Our results are concordant with the observations of Rho & Petre (1998), who find that the majority of MM SNRs are found around dense molecular gas.

We have also shown that the choice of x-ray waveband in which the remnant is imaged can play an important role in deducing whether the remnant is in a mixed-morphology stage or not. If soft x-rays are used, a remnant expanding into a dense ISM will not show itself as centre-bright until rather late in its evolution. On the other hand, the same remnant would show a mixed morphology at reasonably early epochs when imaged in hard x-rays. Remnants expanding into a less dense ISM do not appear centre-bright in either soft or hard x-rays until rather late in their evolution. Even at those epochs, the hard x-rays would more likely show a centre-bright structure than soft x-rays.

ACKNOWLEDGEMENTS

The authors warmly acknowledge discussions with R. Benjamin. DSB acknowledges support via NSF grants AST-005569-001 and NSF-PFC grant PHY02-16783. The simulations were performed at UND and NCSA. This work has made use of the NASA Astrophysics Data System abstract database.

REFERENCES

Asplund, M., Grevesse, N., Sauval, A. J., Allende Prieto, C., & Kiselman, D. 2004, *A&A*, 417, 751

Avillez, M. A. & Breitschwerdt, D. 2005, *ApJL*, 634, L65

Balbus, S. A. 1986, *ApJ*, 304, 787

Balbus, S. A. & McKee, C. F. 1982, *ApJ*, 252, 529

Balsara, D., Benjamin, R. A., & Cox, D. P. 2001, *ApJ*, 563, 800

Balsara, D. S. 1998a, *ApJS*, 116, 119

—. 1998b, *ApJS*, 116, 133

—. 2001, *Journal of Computational Physics*, 174, 614

—. 2004, *ApJS*, 151, 149

Balsara, D. S. & Kim, J. 2005, *ApJ*, 634, 390

Balsara, D. S., Kim, J., Mac Low, M.-M., & Mathews, G. J. 2004, *ApJ*, 617, 339

Balsara, D. S. & Spicer, D. 1999a, *Journal of Computational Physics*, 148, 133

Balsara, D. S. & Spicer, D. S. 1999b, *Journal of Computational Physics*, 149, 270

Begelman, M. C. & McKee, C. F. 1990, *ApJ*, 358, 375

Benjamin, R. A., Benson, B. A., & Cox, D. P. 2001, *ApJL*, 554, L225

Borkowski, K. J., Balbus, S. A., & Fristrom, C. C. 1990, *ApJ*, 355, 501

Cioffi, D. F., McKee, C. F., & Bertschinger, E. 1988, *ApJ*, 334, 252

Clarke, D. A., Burns, J. O., & Norman, M. L. 1989, *ApJ*, 342, 700

Cowie, L. L. & McKee, C. F. 1977, *ApJ*, 211, 135

Cox, D. P., Shelton, R. L., Maciejewski, W., Smith, R. K., Plewa, T., Pawl, A., & Różyczka, M. 1999, *ApJ*, 524, 179

de Avillez, M. A. & Breitschwerdt, D. 2004, *A&A*, 425, 899

Field, G. B. 1965, *ApJ*, 142, 531

Flanagan, K. A., Canizares, C. R., Dewey, D., Houck, J. C., Fredericks, A. C., Schattenburg, M. L., Markert, T. H., & Davis, D. S. 2004, *ApJ*, 605, 230

Frail, D. A., Goss, W. M., Reynoso, E. M., Giacani, E. B., Green, A. J., & Otrupcek, R. 1996, *AJ*, 111, 1651

Gaetz, T. J., Butt, Y. M., Edgar, R. J., Eriksen, K. A., Plucinsky, P. P., Schlegel, E. M., & Smith, R. K. 2000, *ApJL*, 534, L47

Jones, T. W. et al. 1998, *PASP*, 110, 125

Jun, B.-I. & Jones, T. W. 1999, *ApJ*, 511, 774

Kawasaki, M., Ozaki, M., Nagase, F., Inoue, H., & Petre, R. 2005, *ApJ*, 631, 935

Kim, J., Balsara, D., & Mac Low, M.-M. 2001, *Journal of Korean Astronomical Society*, 34, 333

Koo, B.-C. & Moon, D.-S. 1997, *ApJ*, 485, 263

Korpi, M. J., Brandenburg, A., Shukurov, A., Tuominen, I., & Nordlund, Å. 1999, *ApJL*, 514, L99

Mac Low, M.-M., Balsara, D. S., Kim, J., & Avillez, M. A. 2005, *ApJ*, 626, 864

MacDonald, J. & Bailey, M. E. 1981, *MNRAS*, 197, 995

Mazzotta, P., Mazzitelli, G., Colafrancesco, S., & Vittorio, N. 1998, *A&AS*, 133, 403

McKee, C. F. & Ostriker, J. P. 1977, *ApJ*, 218, 148

Oegerle, W. R. e. a. 2005, *ApJ*, 622, 377

Rasmussen, A. P., Behar, E., Kahn, S. M., den Herder, J. W., & van der Heyden, K. 2001, *A&A*, 365, L231

Raymond, J. C. & Smith, B. W. 1977, *ApJS*, 35, 419

Reach, W. T. & Rho, J. 1996, *A&A*, 315, L277

Rho, J. & Petre, R. 1998, *ApJL*, 503, L167+

Roe, P. L. & Balsara, D. S. 1996, *SIAM Journal on Applied Mathematics*, 56, 57

Savage, B. D. & Lehner, N. 2006, *ApJS*, 162, 134

Sedov, L. I. 1959, *Similarity and Dimensional Methods in Mechanics (Similarity and Dimensional Methods in Mechanics)*, New York: Academic Press, 1959

Shelton, R. L., Cox, D. P., Maciejewski, W., Smith, R. K., Plewa, T., Pawl, A., & Różyczka, M. 1999, *ApJ*, 524, 192

Shull, J. M. & Slavin, J. D. 1994, *ApJ*, 427, 784

Slavin, J. D. & Cox, D. P. 1992, *ApJ*, 392, 131

—. 1993, *ApJ*, 417, 187

Smith, R. K., Brickhouse, N. S., Liedahl, D. A., & Raymond, J. C. 2001, *ApJL*, 556, L91

Spitzer, L. 1956, *Physics of Fully Ionized Gases (Physics of Fully Ionized Gases)*, New York: Interscience Publishers, 1956

Tilley, D. A. & Balsara, D. S. 2006, Submitted to *ApJL*

van der Heyden, K. J., Behar, E., Vink, J., Rasmussen, A. P., Kaastra, J. S., Bleeker, J. A. M., Kahn, S. M., &

Mewe, R. 2002, A&A, 392, 955
Vedder, P. W., Canizares, C. R., Markert, T. H., & Pradhan, A. K. 1986, ApJ, 307, 269
Velázquez, P. F., Martinell, J. J., Raga, A. C., & Giacani, E. B. 2004, ApJ, 601, 885
Weiler, K. W. & Sramek, R. A. 1988, ARA&A, 26, 295
White, R. L. & Long, K. S. 1991, ApJ, 373, 543
Woltjer, L. 1972, ARA&A, 10, 129
Yao, Y. & Wang, Q. D. 2005, ApJ, 624, 751